Desalination and Water Treatment
www.deswater.com

doi: 10.1080/19443994.2015.1040468

57 (2016) 10776–10789
May

Taylor & Francis
Taylor & Francis Group

Removal of hexavalent chromium from aqueous solutions by use of chemically modified sour cherry stones

M. Gheju[a,*], I. Balcu[b], P. Jurchescu[a]

[a]*Faculty of Industrial Chemistry and Environmental Engineering, Politehnica University of Timisoara, Bd. V. Parvan Nr. 6, Timisoara 300223, Romania, Tel. +40 256 404185; email: marius.gheju@upt.ro (M. Gheju), Tel. +40 256 403063; email: petru.ionut_jurchescu@yahoo.com (P. Jurchescu)*

[b]*National Institute for Research and Development in Electrochemistry and Condensed Matter, Str. Dr. Aurel Paunescu Podeanu Nr. 144, Timisoara 300587, Romania, Tel. +40 256 222119; email: ionel_balcu@yahoo.com*

Received 30 November 2014; Accepted 8 April 2015

ABSTRACT

A new adsorbent for Cr(VI) removal was prepared from sour cherry stones, by treatment with H_2SO_4 (12–96%). Adsorbent properties were characterized by means of Fourier transform infrared spectroscopy, scanning electron microscopy coupled with energy dispersive X-ray spectroscopy, specific surface area, point of zero charge, iodine number, and analysis of surface functional groups. Surface area increased from 225.5 to 484.7 $m^2\ g^{-1}$, point of zero charge decreased from 6.0 to 3.2, iodine number increased from 4 to 80, total amount of surface acidic groups increased from 1.12 to 2.3 mmol g^{-1} and adsorption capacity increased from 0.53 to 5.27 mg g^{-1}, with increasing H_2SO_4 concentration from 0 to 96%. The pseudo-first- and pseudo-second-order kinetic models have been used to analyze the kinetics of the adsorption; it was found that kinetic experimental data were successfully fitted by the pseudo-first-order model. Equilibrium data were mathematically interpreted by applying the Langmuir, Freundlich, and Dubinin–Radushkevich models; the results indicate that Freundlich model provides the best correlation. Negative values of Gibbs free energy suggest an endothermic and spontaneous adsorption process. The mechanism of Cr(VI) removal involves adsorption of Cr(VI) followed by its partial reduction to Cr(III). Analysis of thermodynamic parameters, coupled with modeling of experimental data with two different intraparticle diffusion models, revealed that binding of Cr(VI) occurred via physisorption, while the rate-limiting step was film diffusion. On the basis of present study, it can be concluded that sour cherry could be suitable adsorbents for the removal of Cr(VI) from polluted waters.

Keywords: Hexavalent chromium; Adsorbent; Waste reuse; Water treatment

1. Introduction

Chromium is an important heavy metal, widely used in various industries such as wood preserving, leather tanning, metal plating, metallurgy, pigment production, chemical manufacturing, and textile dyeing [1]. It may be present in the aquatic environment predominantly in two main valence states, trivalent chromium (Cr(III)), and hexavalent chromium (Cr(VI)), characterized by different chemical

*Corresponding author.

and toxicological properties. Under environmental relevant pH conditions, Cr(III) is relatively insoluble, while Cr(VI) is highly soluble. Cr(VI) is highly toxic to all living organisms and a well-known human carcinogen. In contrast, Cr(III) is up to 1,000 times less toxic than Cr(VI) and, in small amounts, an essential micronutrient for the human metabolism [2]. Hence, it is imperative to reduce the levels of Cr(VI) in wastewaters before discharging into environment. In the same time, water treatment technologies should be not only efficient, but also affordable, especially for communities with low-income [3]. Therefore, great attention has been paid in the last years to the use of cheap and abundant industrial, domestic, or agricultural wastes/byproducts, as sorbents for environmental pollution control [4–10]. Such materials may be used especially when treatment of large volume of diluted solutions is required, because their cost is much lower than of commercial adsorbents [5,11]. Generally, activated carbons are prepared from precursors typically through two routes: physical and/or chemical activation. The latter is often preferred due to several advantages, including: (1) single activation step, (2) lower treatment temperature, (3) shorter activation time, (4) higher carbon yields, (5) well-controlled microporosity, and (6) larger surface area of resulted adsorbents [5,7–9,12]. World production of sour cherries has been relatively stable over the last years, at 1.1–1.2 million tons, with Europe counting for over 65% of the total world production [13,14]. While sweet cherries are mainly consumed fresh, sour cherries are generally consumed after processing into various products, such as jam, wine, juice, dried fruit, candy, and other processed products [15]. Therefore, sour cherry stones are an abundant waste, generated in specific locations, from where it could be easily collected as alternative precursor for the commercial activated carbon production. Nevertheless, reports on adsorptive properties of cherry stones are few. One recent study has shown that sour cherry stones are an attractive source of high porosity carbons, with yields similar to those reported for other fruit stones [16]. To the best of our knowledge, removal of Cr(VI) with adsorbents derived from this precursor has not been researched yet. The objective of this study was to explore the ability of a new adsorbent, prepared from sour cherry (*Prunus cerasus*) stones by chemical treatment with H_2SO_4, to remove Cr(VI) from aqueous solutions. Porosity and surface chemistry of prepared adsorbents was investigated and the effects of H_2SO_4 concentration on kinetics, thermodynamics, and mechanism of Cr(VI) removal were evaluated.

2. Materials and methods

2.1. Materials

A stock solution of Cr(VI) 1,000 mg L^{-1} was prepared by dissolving 2.829 g of $K_2Cr_2O_7$ in 1 L distilled water. The working solution, with a concentration of 2 mg L^{-1}, was prepared by appropriate dilution of stock solution. The pH of working Cr(VI) solution was adjusted to 2.1 by addition of H_2SO_4 96%. Only analytic grade chemical reagents were used.

2.2. Treatment of cherry stones

The collected stones were washed with distilled water, air-dried at room temperature, and crushed in an electric mixer. Thirty grams of stone-powder (SP) were then added to 100 mL H_2SO_4 solution with concentrations of 12, 24, 48, and 96%, and allowed to react for a period of 24 h. The resultant materials, hereinafter referred to as SP12, SP24, SP48, and SP96, were washed with distilled water until constant pH and dried in an oven at 90˚C for 24 h. After cooling, the materials were ground and sieved to particles size 0.3–1.25 mm and further used for the experiments. One control material (SP0) was similarly prepared, using distilled water instead of H_2SO_4 solution.

2.3. Experimental procedure

Batch equilibrium experiments were conducted by adding various amounts of adsorbent to 300 mL Erlenmeyer flasks containing 100 mL working Cr(VI) solution. Preliminary trials (data not shown) indicated that equilibrium was reached after 24 h; therefore, sealed flasks were continuously mixed 24 h at 150 oscillations per minute in a Julabo SW22 shaker, at room temperature (22˚C). Then, solutions were filtered and analyzed for Cr(VI) concentration. Kinetic adsorption experiments were carried out at room temperature (22˚C) in a 1.5 L Berzelius flask, by introducing 2 g of adsorbent into 1,000 mL working Cr(VI) solution. The solution was continuously and vigorously (200 rpm) mixed using an overhead Heidolph stirrer. Samples were taken at preset time intervals, filtered, and analyzed for Cr(VI) and Cr(total).

2.4. Analytical procedure

Cr(VI) concentration in the filtrate was analyzed by the 1,5-diphenylcarbazide method, using a Jasco V 530 spectrophotometer. Cr(total) was determined by oxidizing any Cr(III) with $KMnO_4$, followed by analysis

as Cr(VI); Cr(III) was then determined from the difference between Cr(total) and Cr(VI) (Cr(total) = Cr(III) + Cr(VI)) [17]. The adsorption capacity at time t q_t (mg g^{-1}) and the equilibrium adsorption capacity q_e (mg g^{-1}) were calculated as follows:

$$q_t = \frac{(C_0 - C_t)V}{M} \quad (1)$$

$$q_e = \frac{(C_0 - C_e)V}{M} \quad (2)$$

where M (g) is the mass of adsorbent used in the kinetic experiments, C_e (mg L^{-1}) the equilibrium concentration of Cr(VI), C_t (mg L^{-1}) the Cr(VI) concentration at time t, C_0 (mg L^{-1}) the initial concentration of Cr(VI), and V (L) the volume of Cr(VI) solution used in the kinetic experiments. The pH of solutions was measured using an Inolab pH-meter, calibrated with pH 4 and 7 standard buffers. Scanning electron microscopy (SEM)—energy dispersive angle X-ray spectrometry (EDX) was employed to investigate the morphology and chemical composition of adsorbents, using an Inspect S scanning electron microscope (FEI, Holland) coupled with a GENESIS XM 2i EDX. The FT-IR spectrum of the sample was recorded using a Perkin Elmer spectrophotometer operating in the range of 4,000–400 cm^{-1}, using pellets prepared by mixing and pressing a given sample with KBr. The presence of functional groups was quantified by the Boehm method [18–20]. Point of zero charge (pH_{pzc}) was determined using the pH drift method [20]. Total specific surface area (SSA) was estimated following the ethylene glycol monoethyl ether method [21]. The iodine number (I_n) was determined using the sodium thiosulfate volumetric method, according to ASTM D4607–94 Standard Test Method [22].

3. Results and discussion

3.1. Adsorbent characterization

To ensure conciseness and clarity of this article, the results of FT-IR and SEM analysis are shown and discussed only for three relevant adsorbents: SP0, SP24, and SP96. The FT-IR spectra of adsorbents are illustrated in Figs. 1 and 2, and further interpreted according to literature [23–25]. The broadband around 3,450 cm^{-1} is assigned to O–H stretching, indicating the presence of hydrogen-bonded hydroxyl groups. Peaks observed near 2,930 and 2,850 cm^{-1} can be assigned to the stretching vibration of saturated aliphatic C–H bonds; furthermore, bands at 1,456, 1,430, 1,373, and 1,336 cm^{-1} are referred to bending vibrations of C–H bond in saturated aliphatic. Adsorption bands around 2,350 and 667 cm^{-1} are attributable to CO_2 in the laboratory atmosphere. The band at 1,745 cm^{-1} is indicative for the C=O group stretching, typical for esters; additionally, the peak observed around 1,660 cm^{-1} can be referred to carboxylic and ketonic C=O groups conjugated with aromatic rings or double bonds. Vibrations centered on 1,510 cm^{-1} are indicative of aromatic ring stretch; however, lack of strong bands in 900–650 cm^{-1} suggests that aromatics are sparse. Absorption bands located at 1,045 are caused by C–O stretching vibrations in alkoxy groups. Peaks at 1,160 and 1,242 cm^{-1} are referred to C–O stretching vibrations in acyl groups. The peak at 1,200 cm^{-1}, visible only after treatment with H_2SO_4 96%, may be attributed to $-OSO_3^-$ groups. These results are in accord with previous studies which have reported the presence of vegetable acids, fatty acids, polyphenols, flavonoids, anthocyanidins, tocotrienols, and tocopherol-like components in kernels of sour cherries [26]. Changes in intensity and shift in position of the peaks could be observed when comparing the spectra of raw and acid-treated adsorbents. Most important differences are in the area of hydroxyl and carbonyl group vibrations, suggesting that they were the most affected by the acid treatment. Additionally, the peak at 1,200 cm^{-1} was noticed only after treatment with H_2SO_4 96%, and may be ascribed to OSO_3^- groups. Differences can be seen also when comparing the spectra of un-reacted and exhausted adsorbents, indicating that protonated acidic groups were involved in binding of Cr(VI).

SEM micrographs of selected adsorbents are illustrated in Fig. 3. Visual examination of the SP0 and SP24 micrographs shows the existence of two types of macropores, with sizes of 30–50 μm and 1–2 μm. Instead, the surface of SP96 was covered by smaller macropores, with sizes of 10–30 μm and <1 μm; since the surface area per unit mass increases as pore size decreases, it is expected that the surface area of the adsorbents will increase in the following order: SP0 < SP24 < SP96. The surface of SP0 and SP24 showed little difference after reaction with Cr(VI); in contrast, the surface of SP96 became more heterogeneous and with a rugged morphology after reaction with Cr(VI). This may indicate that intensity of surface interactions between adsorbent and Cr(VI) is much greater for SP96 than for SP24 or SP0, leading to oxidation of the organic matter from the structure of SP96.

The results of EDX analysis are summarized in Table 1. With increasing concentration of H_2SO_4, carbon concentration increases while oxygen concentration decreases; this phenomenon is due to treatment

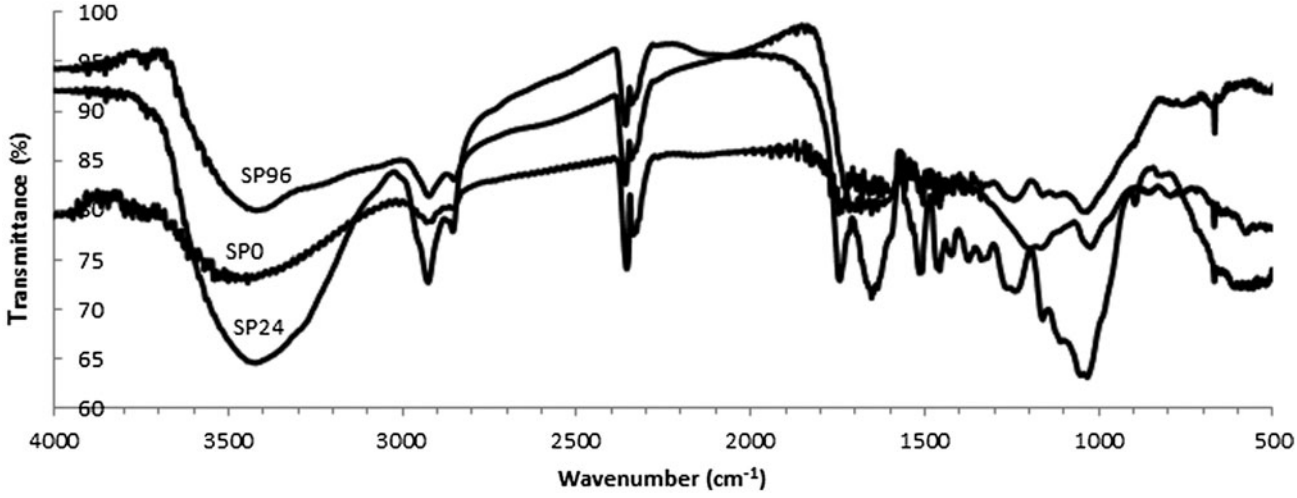

Fig. 1. FT-IR spectra of un-reacted adsorbents.

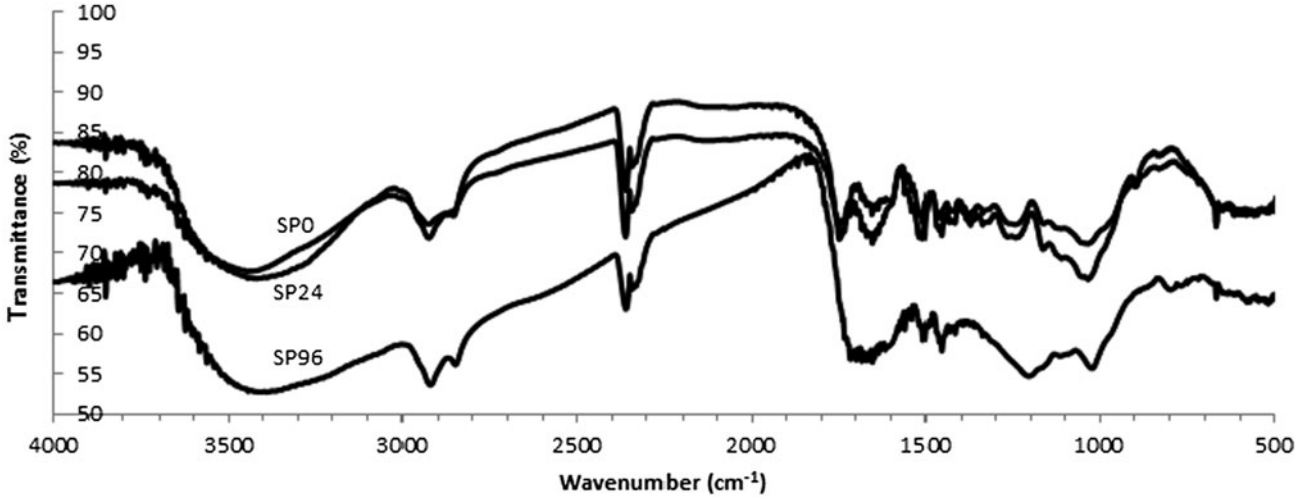

Fig. 2. FT-IR spectra of exhausted adsorbents.

with H_2SO_4, which is an excellent dehydrating agent and can degrade organic precursors to elemental carbon [27]. The composition of the acid-treated adsorbents reveals also the appearance of sulfur, which is certainly the result of contact with H_2SO_4. This confirms the results of the FT-IR analysis which suggests the presence of sulfur-containing groups in acid-treated adsorbent. The spectra of the exhausted adsorbents revealed an additional chromium signal, indicating the binding of the metal to the surface of the sorbent. Chromium concentration in exhausted adsorbents decreased in the following order: SP96 > SP48 > SP24 > SP12 > SP0; hence, the more acidic the conditions of treatment, the higher the Cr (VI) removal efficiency of the resulted adsorbent.

The iodine number (I_n) is a technique that may be used to assess the adsorption capacity and porosity of adsorbent materials [28]. It is defined as the number of milligrams of iodine adsorbed by 1.0 g of adsorbent, when the iodine concentration of the residual filtrate is 0.02 N [22]. Even though I_n does not necessarily provide a measure of the adsorbent ability to retain other species, it still can be used as an approximation for surface area and microporosity of adsorbents [22,28]. As presented in Table 1, both I_n and SSA increased with increasing H_2SO_4 concentration used for the treatment process. This may be ascribed to H_2SO_4 ability to act as dehydrating agent, causing the adsorbent to swell and opening the pores [27]. Therefore, these results show an

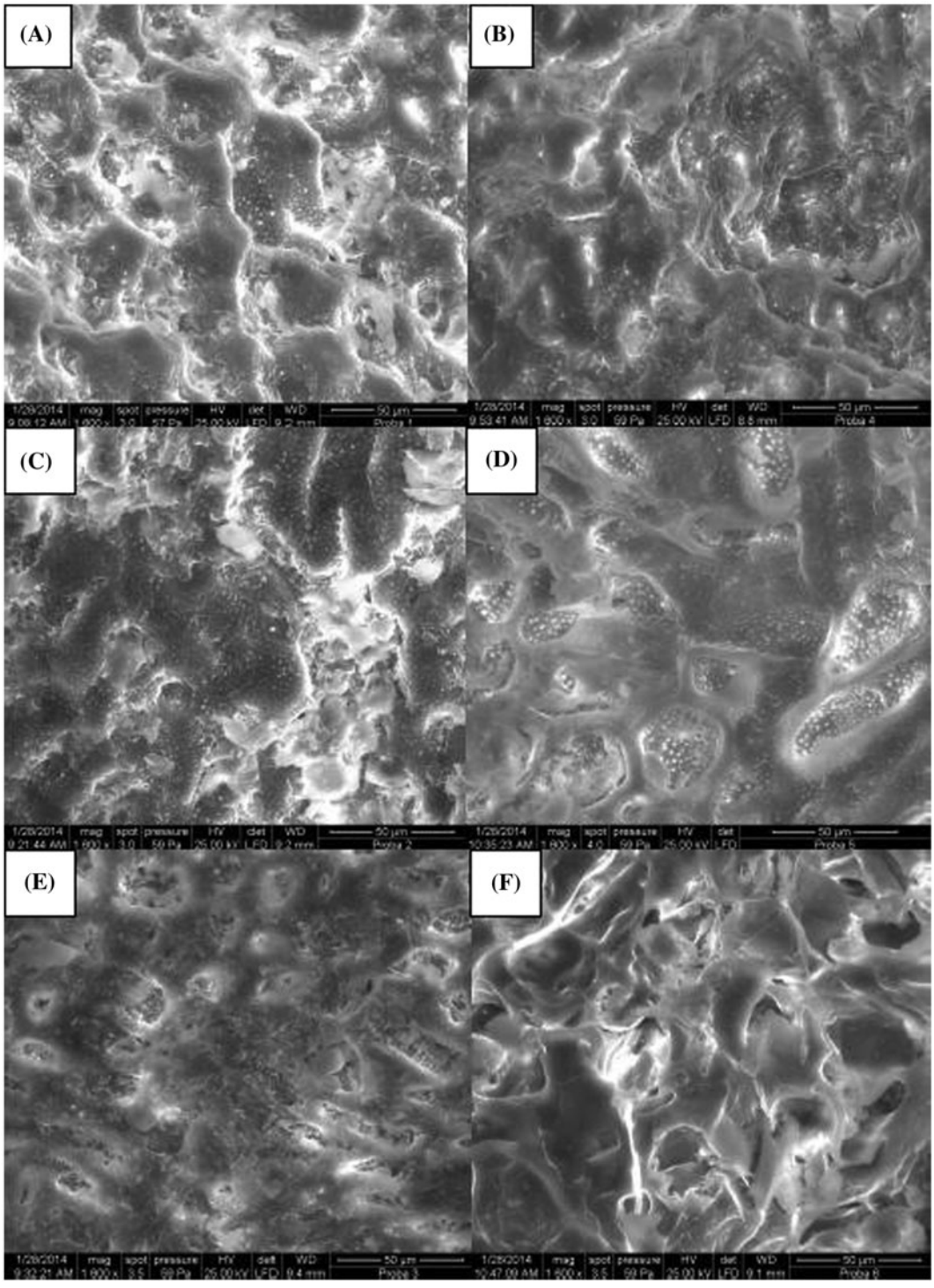

Fig. 3. SEM micrographs of prepared adsorbents: A—un-reacted SP0, B—exhausted SP0, C—un-reacted SP24, D—exhausted SP24, E—un-reacted SP96, F—exhausted SP96.

improvement of both surface area and porosity, as a result of acid treatment, supporting conclusions of SEM analysis.

The results of Boehm titration (Table 1) showed that acid treatment increased the total amount of acidic groups; in contrast, basic groups completely

Table 1
Surface characteristics and element composition (wt%) of studied adsorbents

		SP0	SP12	SP24	SP48	SP96
SSA ($m^2\ g^{-1}$)		225.5	231.5	244.2	249.2	484.7
I_n (mg g^{-1})		6	20	36	40	80
pH_{pzc}		6.0	4.7	4.6	3.2	2.7
Acidic groups (mmol g^{-1})	Carboxyl	0.05	0.15	0.27	0.47	1.5
	Lactone	0.30	0.25	0.13	0.18	0.5
	Phenol	0.77	0.77	0.80	0.77	0.3
	Total	1.12	1.17	1.20	1.42	2.3
Total basic groups (mmol g^{-1})		0.07	0	0	0	0
C	Un-reacted	65.57	66.40	67.68	69.63	73.04
	Exhausted	65.59	66.12	66.10	69.11	73.46
O	Un-reacted	34.11	32.55	31.64	28.15	25.05
	Exhausted	34.09	32.98	33.14	27.75	24.10
S	Un-reacted	NA	0.17	0.35	1.02	1.79
	Exhausted	NA	0.15	0.33	0.94	1.84
Al	Un-reacted	0.32	0.33	0.33	0.24	0.12
	Exhausted	0.32	0.33	0.32	0.22	0.26
Cr	Un-reacted	NA	NA	NA	NA	NA
	Exhausted	NA	0.10	0.11	0.19	0.34

NA—not available.

disappeared after treatment. This is in accord with the values of pH_{pzc} (Table 1) which decreased from 6.0 (SP0) to 2.7 (SP96). Since protonated acidic groups are responsible for the binding of anionic species, acidic treatment seems to be an effective way to improve adsorption capacity of SP toward Cr(VI).

3.2. Kinetic analyses

Fig. 4 illustrates the influence of concentration of H_2SO_4 used in the treatment process, on the kinetics of Cr(VI) removal. It is shown that rate of Cr(VI) removal increased with increasing concentration of H_2SO_4; however, the most significant improvement was achieved only by increasing the concentration of H_2SO_4 from 48 to 96%. For all prepared adsorbents (SP0–SP96), the process proceeded in two steps: the first one, characterized by a high removal rate, followed by a second phase, much slower. This phenomenon may be attributed to the decrease of available active sites on adsorbent surface as time progress.

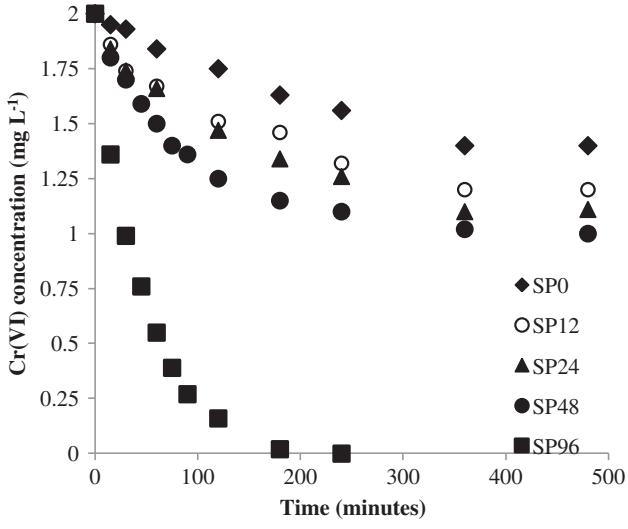

Fig. 4. Effect of H_2SO_4 concentration on Cr(VI) adsorption.

In this work, the pseudo first-order and the pseudo second-order kinetic models have been used to analyze the kinetics of the adsorption. The experimental data was fitted to the linearized forms of the two models, expressed in the form of Eq. (3) (pseudo-first-order) and Eq. (4) (pseudo-second-order) [29–31]:

$$\log\left(q_e - q_t\right) = \log q_e - \frac{k_1}{2,303}t \tag{3}$$

$$\frac{t}{q_t} = \frac{1}{k_2 q_e^2} + \frac{t}{q_e} \tag{4}$$

where q_e (mg g^{-1}) is the equilibrium adsorption capacity, q_t (mg g^{-1}) is the adsorption capacity at time t, k_1 (min^{-1}) and k_2 (g mg^{-1} min^{-1}) are the pseudo-first-order and, respectively, pseudo second-order adsorption rate coefficients. The plot of $\log(q_e - q_t)$ vs. t was a straight line, with slope and intercept equal

to k_1 and q_e, respectively (Fig. 5). Similarly, the plot of t/q_t vs. t enables the k_2 and q_e to be determined from intercept and slope, respectively (Fig. 6). The calculated rate coefficients and the statistical fits of the experimental data to Eqs. (3) and (4) are summarized in Table 2.

Based on the correlation coefficients, it was concluded that experimental data was best described by the pseudo-first-order model, for all investigated adsorbents. This may suggest that interactions in the solution are reversible and only dependent on the number of metal ions present at the specific time [31,32]. The q_e values predicted by the pseudo-first-order model are in better agreement with experimental data than q_e values resulted from the pseudo-second-order equation (Fig. S1), which confirms the pseudo-first-order nature of the sorption process. Table 2 also shows that rate of Cr(VI) adsorption increases with increasing the acidity of the H_2SO_4 treatment solution; this can be explained by considering the increase of the number of positively charged adsorption centers with increasing concentration of H_2SO_4 used in the treatment process (Table 1).

3.3. Adsorption isotherms

The experimental data of adsorption equilibrium was mathematically interpreted by applying three different models, namely, Langmuir, Freundlich, and Dubinin–Radushkevich. The Langmuir model assumes

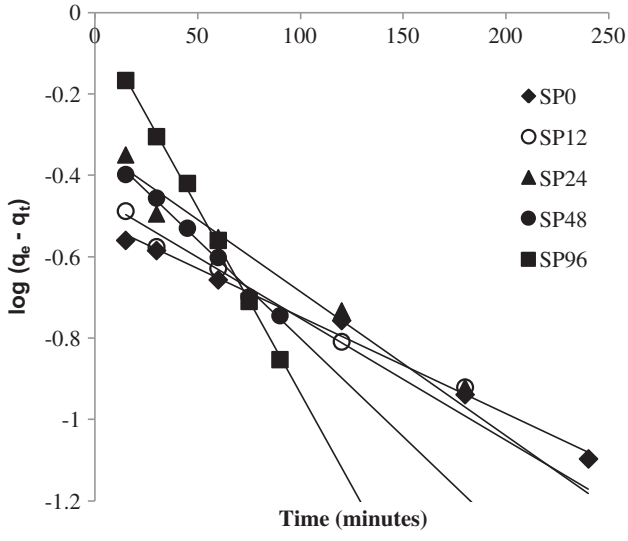

Fig. 5. Linearized pseudo-first-order plots for Cr(VI) adsorption.

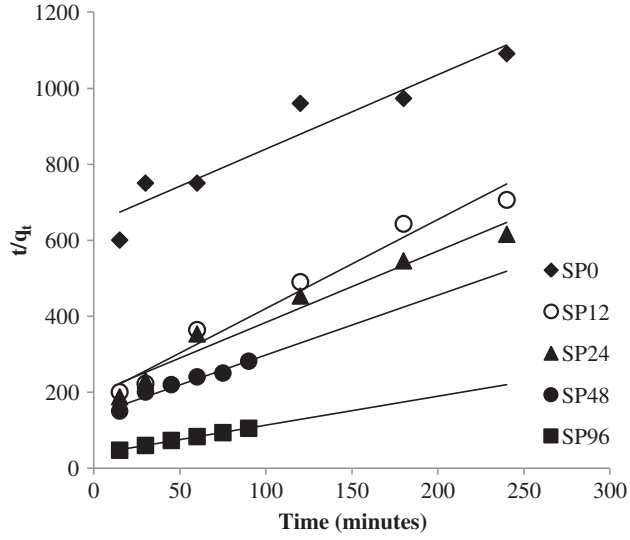

Fig. 6. Linearized pseudo-second-order plots for Cr(VI) adsorption.

that uptake of ions occurs on a homogeneous surface, without any interaction between adsorbed ions, and predicts the existence of monolayer coverage of the adsorbate; the linearized form of Langmuir isotherm is presented in Eq. (5) [33,34]:

$$\frac{1}{q_e} = \frac{1}{q_{max}} + \frac{1}{q_{max} K_L} \frac{1}{C_e} \tag{5}$$

where q_{max} (mg g^{-1}) is the maximum monolayer adsorption capacity, K_L (L mg^{-1}) is the adsorption equilibrium constant, C_e (mg L^{-1}) is the equilibrium concentration of Cr(VI), and q_e (mg g^{-1}) is the amount of Cr(VI) adsorbed at equilibrium. The Freundlich model is an empirical equation which considers that adsorption takes place on a heterogeneous surface, possibly by multilayer adsorption, accompanied by interaction between adsorbed molecules; the linearized form of the Freundlich isotherm is presented in Eq. (6) [33,35]:

$$\log q_e = \log K_f + \frac{1}{n} \log C_e \tag{6}$$

where K_f is a constant related to the maximum adsorption capacity of the adsorbent, $1/n$ stands for the intensity of adsorption, C_e (mg L^{-1}) is the equilibrium concentration of Cr(VI), and q_e (mg g^{-1}) is the amount of Cr(VI) adsorbed at equilibrium. The linearized form of the Dubinin–Radushkevich isotherm is presented in Eq. (7) [31,36]:

Table 2
Pseudo-first-order and pseudo-second-order kinetic parameters of Cr(VI) adsorption

		SP0	SP12	SP24	SP48	SP96
Pseudo-first-order	k_1 (min^{-1})	5.5×10^{-3}	6.9×10^{-3}	8.0×10^{-3}	11.0×10^{-3}	20.9×10^{-3}
	R^2	0.9913	0.9759	0.9822	0.9938	0.9985
Pseudo-second-order	k_2 (g mg^{-1} min^{-1})	5.9×10^{-3}	29.1×10^{-3}	18.2×10^{-3}	17.9×10^{-3}	15.9×10^{-3}
	R^2	0.9082	0.9710	0.9599	0.9498	0.9978

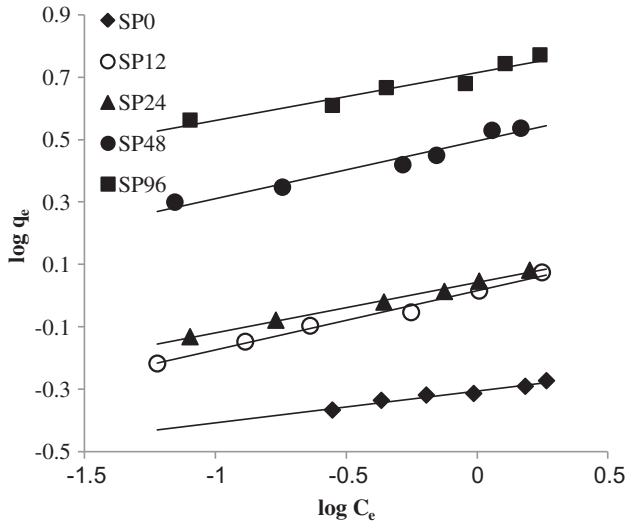

Fig. 7. Linearized Freundlich adsorption isotherms.

$$\ln q_e = \ln q_{max} - \beta\varepsilon^2 \quad (7)$$

where q_{max} (mg g^{-1}) represents the maximum adsorption capacity of the adsorbent, β (mol^2 J^{-2}) is a constant related to the mean free energy of adsorption, q_e (mg g^{-1}) is the amount of Cr(VI) adsorbed at equilibrium, and ε (J^2 mol^{-2}) is the Polanyi adsorption potential, computed as follows:

$$\varepsilon = RT \ln\left(1 + \frac{1}{C_e}\right) \quad (8)$$

where: R (8.314 J mol^{-1} K^{-1}) is the universal gas constant, C_e (mg L^{-1}) is the equilibrium concentration of Cr(VI), and T (K) is the absolute temperature. The mean energy of adsorption was then calculated using the equation:

$$E = \frac{1}{\sqrt{2\beta}} \quad (9)$$

The linearized forms of the three adsorption models were used to evaluate the equilibrium of Cr(VI) adsorption. Freundlich constants K_f and $1/n$ were determined from the slope and intercept of the plot of ln q_e vs. ln C_e (Fig. 7). Langmuir constants q_{max} and K_L were computed from the plot of $1/q_e$ as a function of $1/C_e$ (Fig. 8). Similarly, the plot of ln q_e vs. ε^2 produces a straight line which enables the calculation of Dubinin–Radushkevich constants q_{max} (intercept) and β (slope) (Fig. 9).

Table 3 summarizes the equilibrium adsorption parameters resulted from Langmuir, Freundlich, and Dubinin–Radushkevich isotherms. Freundlich isotherm provided highest correlation coefficients for all adsorbents, which indicate that removal of Cr(VI) was not restricted to the formation of a monolayer and surface of the sorbents is heterogeneous. Examination of Table 3 also shows that adsorption capacity of SP96 was nearly ten times higher than of SP0. In addition, a good correlation was observed between the two constants related to the maximum adsorption capacity, q_{max} and K_f. The increase in affinity of the adsorbents toward Cr(VI) with increasing concentration of H_2SO_4 used for chemical treatment may be attributed to the increase of positively charged functional groups available for anionic chromium species, as resulted from

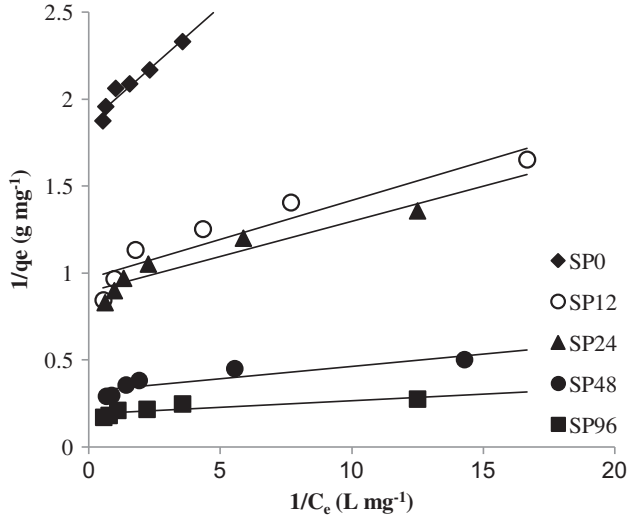

Fig. 8. Linearized Langmuir adsorption isotherms.

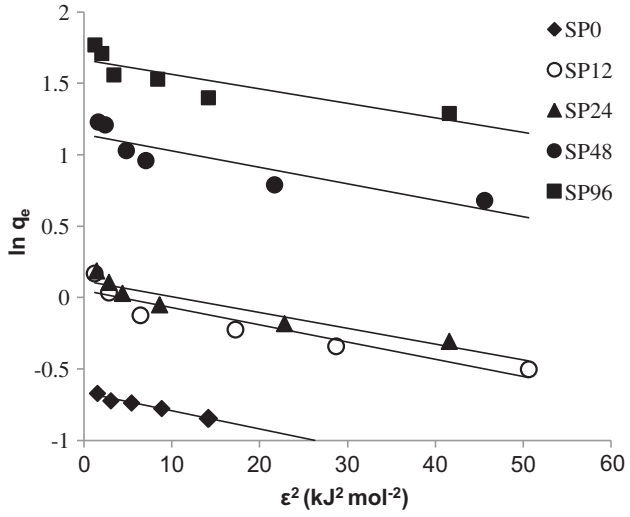

Fig. 9. Linearized Dubinin–Radushkevich adsorption isotherms.

Boehm analysis (Table 1). Comparison of adsorption capacity with literature data is presented in Table S1 [37–46]; since cherry stone powder do not seem to have a very high adsorption capacity, they may be used especially for the treatment of large volume of wastewaters contaminated with low Cr(VI) concentrations. The Freundlich $1/n$ constant may be considered a representation of the affinity of Cr(VI) toward adsorbent. The adsorption process is considered favorable when $0.1 < 1/n < 1.0$; the smaller the value of $1/n$, the higher the intensity of adsorption and the stronger the bonds between the adsorbate and the adsorbent [47,48]. The degree of favorability can be also related to the Langmuir dimensionless separation parameter R_L, defined as follows [33]:

$$R_L = \frac{1}{1 + K_L \cdot C_0} \tag{10}$$

where C_0 (mg/L) is the initial concentration of the Cr(VI) and K_L is the Langmuir constant. The adsorption process is considered favorable when $0 < R_L < 1$ [33]; the R_L degrees tended toward zero for the completely ideal irreversible case, and toward unity, for the completely reversible case [7]. Since values of both $1/n$ and R_L were found to be in between 0 and 1 (Table 3), it demonstrate that sorption of Cr(VI) was favorable under studied conditions.

3.4. Thermodynamic parameters

Values of Gibbs free energy of adsorption (ΔG), enthalpy change (ΔH), entropy change (ΔS), and activation energy (E_a) were computed by interpreting results of experiments conducted at 6, 22, and 32 °C. The equilibrium constant K_c (L g^{-1}) of the adsorption process was evaluated using the following relationship [49]:

$$K_c = \frac{C^e_{ads}}{C^e_{aq}} \tag{11}$$

where C^e_{ads} is the equilibrium concentration of Cr(VI) on the adsorbent (mg g^{-1}) and C^e_{aq} is the equilibrium concentration of Cr(VI) in the aqueous solution (mg L^{-1}). Then, values of ΔG as a function of temperature were determined using van't Hoff equation:

$$\Delta G = -R \cdot T \cdot \ln K_c \tag{12}$$

where K_c (L mol^{-1}) is the equilibrium constant, R (8.314 J mol^{-1} K^{-1}) is the universal gas constant, and T (K) is the absolute temperature. Subsequently, ΔH and ΔS were computed from the slope and intercept of the plot of ΔG vs. T (Fig. S2, supplementary material), according to Gibbs isotherm:

$$\Delta G = \Delta H - T \cdot \Delta S \tag{13}$$

The activation energy of the adsorption process was estimated using the logarithmic form of the Arrhenius equation [50]:

$$\ln k = \ln A - \frac{E_a}{RT} \tag{14}$$

where k is the rate constant at temperature T, A is the pre-exponential factor, R (8.314 J mol^{-1} K^{-1}) is the universal gas constant, and T (K) is the absolute temperature. E_a was calculated from the slope of the plot of ln k_1 vs. $1/T$ (Fig. S3, supplementary material). Values of ΔG, ΔH, ΔS, and E_a are listed in Table 4. The negative values of the ΔG suggest that adsorption is spontaneous and feasible; ΔG became more negative with increasing temperature and concentration of H_2SO_4 used in the treatment process, reflecting a much more stable and energetically favorable adsorption of Cr(VI) [51]. The positive values of ΔH indicate an endothermic process, while the positive value of ΔS corresponds to an increased randomness at the solid–solution interface during the adsorption process [52]. Lowest values of E_a were observed for SP96, suggesting a more favorable adsorption process.

Table 3
Freundlich, Langmuir, and Dubinin–Radushkevich equilibrium parameters of Cr(VI) adsorption

		SP0	SP12	SP24	SP48	SP96
Freundlich	K_f	0.49	1.04	1.10	3.12	5.19
	$1/n$	0.10	0.19	0.16	0.18	0.15
	R^2	0.9615	0.9877	0.9944	0.9578	0.9339
Langmuir	q_{max} (mg g^{-1})	0.53	1.03	1.12	3.12	5.27
	K_L (L mg^{-1})	13.95	21.50	22.01	22.54	25.29
	R_L	0.034	0.022	0.022	0.021	0.019
	R^2	0.9390	0.8801	0.8948	0.7930	0.7413
Dubinin–Radushkevich	q_{max} (mg g^{-1})	0.52	1.05	1.11	3.12	5.26
	β (mol^2 kJ^{-2})	1.46×10^{-2}	1.20×10^{-2}	1.10×10^{-2}	1.15×10^{-2}	1.02×10^{-2}
	E (kJ mol^{-1})	5.97	6.45	6.74	6.59	7.00
	R^2	0.9194	0.8760	0.8935	0.8020	0.7415

Table 4
Thermodynamic parameters of Cr(VI) adsorption

	ΔG (kJ mol^{-1})					
	t = 6 °C	t = 22 °C	t = 32 °C	ΔH (kJ mol^{-1})	ΔS (J mol^{-1})	E_a (kJ mol^{-1})
SP0	−5.19	−5.91	−6.29	6.67	42.60	14.10
SP12	−6.22	−7.00	−7.50	7.51	49.20	13.95
SP24	−6.71	−7.50	−8.26	9.70	58.70	13.54
SP48	−7.00	−7.98	−8.62	10.38	62.30	13.26
SP96	−8.70	−10.18	−12.16	27.55	129.30	9.24

3.5. Mechanism of Cr(VI) removal

3.5.1. Identifying mechanism of Cr(VI) removal

There are four models for the Cr(VI) removal mechanism when carbon-based adsorbents are involved: (1) anionic adsorption, (2) adsorption-coupled reduction, (3) anionic and cationic adsorption, and (4) reduction and anionic adsorption [6]. Carbon-based organic materials are well-known reductants of Cr(VI) [53]:

$$2HCrO_4^- + 2C + 6H^+ \rightarrow 2Cr^{3+} + 2CO_2 + 4H_2O \quad (15)$$

Therefore, most often, removal of Cr(VI) using carbon-based adsorbents is not a pure anionic adsorption process. It is a complex process which may occur along three parallel pathways: (1) retention of Cr(VI) (via chemical, physical, or ion exchange sorption processes), (2) reduction of Cr(VI) to Cr(III), and (3) retention of Cr(III) (via sorption or precipitation processes). At $pH < pH_{pzc}$ the adsorbent surface will have a net positive charge and sorption of cations is significantly hindered. Hence, we can assume that, at pH 2, retention of Cr(III) via adsorption is negligible. This is in accord with previous works which reported that, under similar pH conditions, no Cr(III) adsorption was observed [54–56]. Furthermore, since at pH 2 the prevalent species of Cr(III) is the highly soluble Cr^{3+} [57], retention of Cr(III) by precipitation is also negligible. In order to have a more detailed understanding on the contribution of adsorption and reduction, concentrations of Cr(III) were analyzed at equilibrium. The results showed that only small amounts of Cr(III) (7.2–13.5% from Cr(initial)) were detected. Thus, we can assume that, under the experimental conditions involved in this study, removal of Cr(VI) occurred through a combined adsorption–reduction process, with reduction having only a minor contribution.

3.5.2. Identifying type of Cr(VI) sorption

Thermodynamic parameters determined in Section 3.4. were used for differentiating between physical, chemical, and ion exchange sorption processes, which may be involved in binding of Cr(VI). The values of Dubinin-Radushkevish mean energy

(5.97–7 kJ mol^{-1}) was below 8 kJ mol^{-1}, suggesting that sorption occurs via physisorption [32]. The magnitude of ΔH (6.67–27.55 kJ mol^{-1}) was smaller than 40 kJ mol^{-1}, also indicating a physical adsorption process [58]. The value of activation energy (9.24–14.10 kJ mol^{-1}) lies within 5–40 kJ mol^{-1}, which is the specific range for physisorption [59]. Therefore, it can be concluded that binding of Cr(VI) occurred via physisorption.

3.5.3. Identifying adsorption limiting step

Adsorption of an adsorbate by a porous adsorbent can be generally described by following consecutive steps: (1) transport of the adsorbate in the bulk of the solution, (2) transport of the adsorbate through the liquid film surrounding the adsorbent particle, to its external surface (film diffusion), (3) transport of the adsorbate from the adsorbent surface into its pores (intraparticle diffusion), and (4) retention of the adsorbate on the interior sites of the pores [7,60]. Usually, in well-mixed batch systems as the one employed in this work, transport in the bulk of the solution does not become rate limiting [60]. Similarly, step (4) is also very rapid and does not normally represent the rate determining step in the uptake of adsorbate [7]. To determine whether film diffusion or intraparticle diffusion is the rate limiting step, the kinetic experimental results were fitted to the Weber and Morris intraparticle diffusion model [61]:

$$q_t = k_{diff} \cdot t^{0.5} + C \tag{16}$$

where q_t (mg g^{-1}) is the adsorption capacity at time t, k_{diff} (mg g^{-1} min$^{-0.5}$) is the intraparticle diffusion rate constant, and C is a constant related to the thickness of the boundary layer. If intraparticle diffusion is the sole rate limiting step, the plot of q_t vs. $t^{0.5}$ should yield a straight line passing through the origin (C=0), with slope k_{diff}; if the line does not intersect the origin (C≠0) or the plot is nonlinear, some other mechanism may also be involved [60,62]. Fig. S4 (supplementary material) depicts the plots obtained for the Weber and Morris model, while Table 5 summarizes the values of k_{diff} and C constants. Even though the correlation coefficients show a relative good linearity of the plots, they do not pass through the origin. Therefore, it appears that the controlling process in the adsorption system was film diffusion. Prediction of the sorption rate-limiting step can also be carried out using the Boyd diffusion model, expressed as [63]:

$$F = \frac{q_t}{q_e} = 1 - \frac{6}{\pi^2}\sum_{n=1}^{\infty}\frac{1}{n^2}\exp\left(-n^2 B_t\right) \tag{17}$$

where F is the fractional attainment of equilibrium at various times, q_t and q_e (mg g^{-1}) are the amounts adsorbed at time t and at equilibrium, and B_t is Boyd's constant. The simplified form of Boyd's model, obtained by Reichenberg after applying the Fourier transform, can be written as follows [64]:

$$B_t = -0.4977 - \ln(1 - F), \quad \text{for } F > 0.85 \tag{18}$$

$$B_t = \left(\sqrt{\pi} - \sqrt{\pi - \pi^2\frac{F}{3}}\right)^2, \quad \text{for } 0.85 > F > 0 \tag{19}$$

In order to assess the nature of rate limiting step, the value of B_t was calculated for each q_t and then plotted against t. If the plot is linear and passes through the origin, intraparticle diffusion is the limiting step; if the plot is nonlinear, or linear but does not pass through the origin, film diffusion controls the adsorption rate [64]. The plots obtained for the Boyd model (Fig. S5, supplementary material) illustrate a bad linearity over the period studied, confirmed by the correlation coefficients (Table 5); moreover, Boyd plots also do not pass through the origin, supporting

Table 5
Diffusion models parameters and diffusion coefficients of Cr(VI) adsorption

	Weber and Morris			Boyd		Diffusion coefficients	
	k_{diff}	C	R^2	Intercept	R^2	D_p (cm^2 s^{-1})	D_f (cm^2 s^{-1})
SP0	0.0171	0.0501	0.9902	0.1209	0.9470	0.8×10^{-8}	0.4×10^{-8}
SP12	0.0215	0.0025	0.9890	0.1080	0.9492	1.2×10^{-8}	0.8×10^{-8}
SP24	0.0264	0.0229	0.9970	0.1659	0.9500	1.3×10^{-8}	0.9×10^{-8}
SP48	0.0411	0.0661	0.9928	0.1144	0.9764	2.1×10^{-8}	1.5×10^{-8}
SP96	0.0967	0.0364	0.9944	0.2365	0.9882	3.1×10^{-8}	4.8×10^{-8}

film diffusion as the rate limiting step. The pore diffusion coefficient (D_p) and the film diffusion coefficient (D_f) were computed also according to Eqs. (20) and (21), assuming spherical geometry for the sorbent particles [5,65]:

$$D_p = 0.03 \cdot \frac{r^2}{t_{1/2}} \quad (20)$$

$$D_f = 0.23 \cdot \frac{r\varepsilon}{t_{1/2}} \cdot \frac{q_e}{C_0} \quad (21)$$

where r (cm) is the radius of the sorbent particle, ε the film thickness (assumed 10^{-3} cm), q_e (mg g^{-1}) the amount of metal sorbed at equilibrium, C_0 (mg L^{-1}) the initial concentration, and $t_{1/2}$ (s) the time for half sorption, required to uptake half of the amount of Cr(VI) adsorbed at equilibrium. The value of the D_f should be in the range of 10^{-6}–10^{-8} cm^2 s^{-1} if film diffusion is the rate-determining step, while the D_p value should be in the range of 10^{-11}–10^{-13} cm^2 s^{-1} if pore diffusion is the rate limiting step [5]. Table 5 illustrates the dependence between diffusion coefficients and the concentration of H_2SO_4 used in the treatment process. Two important conclusions can be drawn from the examination of this Table 1 since both D_f and D_p coefficients are in the range of 0.4–4.8 × 10^{-8}, it seems that adsorption of Cr(VI) was controlled by the film diffusion process, and (2) values of D_p and D_f are increasing with the increase of H_2SO_4 concentration used for the treatment process, suggesting that diffusion process was favorably affected by the acid treatment: the higher the concentration of H_2SO_4, the higher the diffusion coefficients and the lower the resistance to diffusion. Summarizing, the analyses of D_f and D_p diffusion coefficients corroborate the conclusions from both Weber–Morris and Boyd models, that film diffusion was the rate limiting step in the studied adsorption system.

4. Conclusions

Sour cherry stones were used as adsorbents to remove Cr(VI) from aqueous solutions. Adsorption capacity increased after acid treatment from 0.53 mg g^{-1} (SP0) to 5.27 mg g^{-1} (SP96) due to improvement of surface area, microporosity, and surface chemistry. The best fit of equilibrium data was obtained with the Freundlich isotherm. Adsorption kinetics was most accurately described by the pseudo-first-order model. A possible adsorption-coupled reduction mechanism for Cr(VI) removal has been suggested, with physisorption the major mechanism responsible for Cr(VI) adsorption and film diffusion the rate-limiting step. The present study shows that sour cherry stones are an effective new adsorbent for removing Cr(VI) from polluted waters.

Supplementary material

The supplementary material for this paper is available online at http://dx.doi.10.1080/19443994.2015.1040468.

Acknowledgments

We thank two anonymous reviewers for their insightful comments that helped to improve the final version of the manuscript.

References

[1] R. Saha, R. Nandi, B. Saha, Sources and toxicity of hexavalent chromium, J. Coord. Chem. 64 (2011) 1782–1806.
[2] M. Gheju, Hexavalent chromium reduction with zero-valent iron (ZVI) in aquatic systems, Water Air Soil Pollut. 222 (2011) 103–148.
[3] C. Noubactep, Metallic iron for safe drinking water worldwide, Chem. Eng. J. 165 (2010) 740–749.
[4] V.K. Gupta, Suhas, Application of low-cost adsorbents for dye removal—A review, J. Environ. Manage. 90 (2009) 2313–2342.
[5] V.K. Gupta, P.J.M. Carrott, M.M.L. Ribeiro Carrott, Suhas, Low-cost adsorbents: Growing approach to wastewater treatment—A review, Crit. Rev. Env. Sci. Technol. 39 (2009) 783–842.
[6] B. Saha, C. Orvig, Biosorbents for hexavalent chromium elimination from industrial and municipal effluents, Coord. Chem. Rev. 254 (2010) 2959–2972.
[7] D. Mohan, C.U. Pittman Jr., Activated carbons and low cost adsorbents for remediation of tri- and hexavalent chromium from water, J. Hazard. Mater. B137 (2006) 762–811.
[8] R.K. Gautam, A. Mudhoo, G. Lofrano, M.C. Chattopadhyaya, Biomass-derived biosorbents for metal ions sequestration: Adsorbent modification and activation methods and adsorbent regeneration, J. Environ. Chem. Eng. 2 (2014) 239–259.
[9] N.M. Nor, L.L. Chung, L.K. Teong, A.R. Mohamed, Synthesis of activated carbon from lignocellulosic biomass and its applications in air pollution control—A review, J. Environ. Chem. Eng. 1 (2013) 658–666.
[10] H.R. Zafarani, M.E. Bahrololoom, C. Noubactep, J. Tashkhourian, Green walnut shell as a new material for removal of Cr(VI) ions from aqueous solutions, Desalin. Water Treat. doi: 10.1080/19443994.2014.917986.
[11] K. Chojnacka, Equilibrium and kinetic modelling of chromium(III) sorption by animal bones, Chemosphere 59 (2005) 315–320.
[12] M. Danish, R. Hashim, M.N.M. Ibrahim, O. Sulaiman, Effect of acidic activating agents on surface area and surface functional groups of activated carbons

produced from *Acacia mangium* wood, J. Anal. Appl. Pyrolysis 104 (2013) 418–425.
[13] A. Montgomery, Sour Cherries in Canada, Canadian Agriculture at a Glance, Statistics Canada Catalogue no. 96-325-X, 2009, pp. 1–9.
[14] Z. Sredojevic, D. Milic, M. Jelocnik, Investment in sweet and sour cherry production and new processing programs in terms of serbian agriculture competitiveness, Petrol. Gas Univ. Ploiesti BULL. Econ. Sci. Ser. LXIII(3) (2011) 37–49.
[15] J. Cao, Q. Jiang, J. Lin, X. Li, C. Sun, K. Chen, Physicochemical characterisation of four cherry species (*Prunus* spp.) grown in China, Food Chem. 173 (2015) 855–863.
[16] D. Angin, Production and characterization of activated carbon from sour cherry stones by zinc chloride, Fuel 115 (2014) 804–811.
[17] APHA, AWWA, WPCF, Standard Methods for the Examination of Water and Wastewater, nineteenth ed., American Public Health Association, Washington, DC, 1995.
[18] S.L. Goertzen, K.D. Theriault, A.M. Oickle, A.C. Tarasuk, H.A. Andreas, Standardization of the Boehm titration. Part I. CO_2 expulsion and endpoint determination, Carbon 48 (2010) 1252–1261.
[19] A.M. Oickle, S.L. Goertzen, K.R. Hopper, Y.O. Abdalla, H.A. Andreas, Standardization of the Boehm titration: Part II. Method of agitation, effect of filtering and dilute titrant, Carbon 48 (2010) 3313–3322.
[20] A. Zach-Maor, R. Semiat, H. Shemer, Synthesis, performance, and modeling of immobilized nano-sized magnetite layer for phosphate removal, J. Colloid Interface Sci. 357 (2011) 440–446.
[21] A.B. Cerato, A.J. Lutenegger, Determination of surface area of fine-grained soils by the ethylene glycol monoethyl ether (EGME) method, Geotech. Test. J. 25 (2002) 314–320.
[22] ASTM D4607-94, Standard Test Method for Determination of Iodine Number of Activated Carbon, ASTM International, West Conshohocken, 2006, pp. 1–5.
[23] J. Coates, Interpretation of infrared spectra, a practical approach, in: R.A. Meyers, Encyclopedia of Analytical Chemistry, John Wiley, Chichester, 2000, pp. 10815–10837.
[24] J.M. Chalmers, Anomalies, artifacts and common errors in using vibrational spectroscopy techniques, in: J.M. Chalmers, P. Griffiths, Handbook of Vibrational Spectroscopy, John Wiley, Chichester, 2002, pp. 2327–2347.
[25] P. Patnaik, Dean's Analytical Chemistry Handbook, McGraw-Hill, New York, NY, 2004.
[26] I. Bak, I. Lekli, B. Juhasz, E. Varga, B. Varga, R. Gesztelyi, L. Szendrei, A. Tosaki, Isolation and analysis of bioactive constituents of sour cherry (*Prunus cerasus*) seed kernel: An emerging functional food, J. Med. Food 13 (2010) 905–910.
[27] M. Olivares-Marin, C. Fernández-González, A. Macías-García, V. Gómez-Serrano, Preparation of activated carbon from cherry stones by physical activation in air. Influence of the chemical carbonisation with H_2SO_4, J. Anal. Appl. Pyrolysis 94 (2012) 131–137.
[28] C. Saka, BET, TG–DTG, FT-IR, SEM, iodine number analysis and preparation of activated carbon from acorn shell by chemical activation with $ZnCl_2$, J. Anal. Appl. Pyrolysis 95 (2012) 21–24.
[29] Y.S. Ho, G. McKay, Pseudo-second order model for sorption processes, Process Biochem. 34 (1999) 451–465.
[30] Y.S. Ho, Review of second-order models for adsorption systems, J. Hazard. Mater. B136 (2006) 681–689.
[31] S.S. Gupta, K.G. Bhattacharyya, Kinetics of adsorption of metal ions on inorganic materials: A review, Adv. Colloid Interface Sci. 162 (2011) 39–58.
[32] K. Srividya, K. Mohanty, Biosorption of hexavalent chromium from aqueous solutions by Catla catla scales: Equilibrium and kinetics studies, Chem. Eng. J. 155 (2009) 666–673.
[33] M. Bansal, D. Singh, V.K. Garg, A comparative study for the removal of hexavalent chromium from aqueous solution by agriculture wastes' carbons, J. Hazard. Mater. 171 (2009) 83–92.
[34] Z.J. Hu, N.X. Wang, J. Tan, J.Q. Chen, W.Y. Zhong, Kinetic and equilibrium of cefradine adsorption onto peanut husk, Desalin. Water Treat. 37 (2012) 160–168.
[35] M.C. Shih, Kinetics of the batch adsorption of methylene blue from aqueous solutions onto rice husk: Effect of acid-modifi ed process and dye concentration, Desalin. Water Treat. 37 (2012) 200–214.
[36] M. Eloussaief, N. Kallel, A. Yaacoubi, M. Benzina, Mineralogical identification, spectroscopic characterization, and potential environmental use of natural clay materials on chromate removal from aqueous solutions, Chem. Eng. J. 168 (2011) 1024–1031.
[37] J.V. Rios, L. Bess-Oberto, K.J. Tiemann, J.L. Gardea-Torresdey, Investigation of metal ion binding by agricultural by-products, in: Proceedings of the 1999 Conference on Hazardous Waste Research, St. Louis, Missouri, 1999, pp. 121–130.
[38] W.T. Tan, S.T. Ooi, C.K. Lee, Removal of Cr(VI) from solution by coconut husk and palm pressed fibers, Environ. Technol. 14 (1993) 277–282.
[39] M. Dakiky, M. Khamis, A. Manassra, M. Mereb, Selective adsorption of chromium(VI) in industrial wastewater using low-cost abundantly available adsorbents, Adv. Environ. Res. 6(4) (2002) 533–540.
[40] D.C. Sharma, C.F. Forster, A preliminary examination into the adsorption of hexavalent chromium using low-cost adsorbents, Bioresour. Technol. 47(3) (1994) 257–264.
[41] N.K. Hamadi, X.D. Chen, M.M. Farid, M.G.Q. Lu, Adsorption kinetics for the removal of chromium (VI) from aqueous solution by adsorbents derived from used tyres and sawdust, Chem. Eng. J. 84 (2001) 95–105.
[42] P.L. Tang, C.K. Lee, K.S. Low, Z. Zainal, Sorption of Cr(VI) and Cu(II) in aqueous solution by ethylenediamine modified rice hull, Environ. Technol. 24 (2003) 1243–1251.
[43] G.H. Pino, L.M.S. de Mesquita, M.L. Torem, G.A.S. Pinto, Biosorption of heavy metals by powder of green coconut shell, Sep. Sci. Technol. 41 (2006) 3141–3153.
[44] D. Mohan, K.P. Singh, V.K. Singh, Removal of hexavalent chromium using low-cost activated carbons derived from agricultural waste materials and activated carbon fabric cloth, Ind. Eng. Chem. Res. 44 (2005) 1027–1042.
[45] G. Cimino, A. Passerini, G. Toscano, Removal of toxic cations and Cr(VI) from aqueous solution by hayelnut shell, Water Res. 34(11) (2000) 2955–2962.

[46] C. Namasivayam, D. Sangeetha, Removal of chromium(VI) by $ZnCl_2$ activated coir pith carbon, Toxicol. Environ. Chem. 88 (2006) 219–233.
[47] E. Malkoc, Y. Nuhoglu, M. Dundar, Adsorption of chromium(VI) on pomace—An olive oil industry waste: Batch and column studies, J. Hazard. Mater. B138 (2006) 142–151.
[48] R. Aravindhan, B. Madhan, J. Raghava Rao, B.U. Nair, T. Ramasami, Bioaccumulation of chromium from tannery wastewater: An approach for chrome recovery and reuse, Environ. Sci. Technol. 38 (2004) 300–306.
[49] T. Karthikeyan, S. Rajgopal, L.R. Miranda, Chromium (VI) adsorption from aqueous solution by *Hevea brasilinesis* sawdust activated carbon, J. Hazard. Mater. B124 (2005) 192–199.
[50] S.S. Baral, S.N. Das, P. Rath, Hexavalent chromium removal from aqueous solution by adsorption on treated sawdust, Biochem. Eng. J. 31 (2006) 216–222.
[51] K.G. Bhattacharyya, S.S. Gupta, Adsorption of chromium(VI) from water by clays, Ind. Eng. Chem. Res. 45 (2006) 7232–7240.
[52] F. Granados-Correa, J. Jimenez-Becerril, Chromium (VI) adsorption on boehmite, J. Hazard. Mater. 162 (2009) 1178–1184.
[53] L. Ying, Y. Qinyan, G. Baoyu, L. Qian, L. Chunling, Adsorption thermodynamic and kinetic studies of dissolved chromium onto humic acids, Colloids Surf., B 65 (2008) 25–29.
[54] M. Dakiky, M. Khamis, A. Manassra, M. Mer'eb, Selective adsorption of chromium(VI) in industrial wastewater using low-cost abundantly available adsorbents, Adv. Environ. Res. 6 (2002) 533–540.
[55] R. Leyva-Ramos, L. Fuentes-Rubio, R.M. Guerrero-Coronado, J. Mendoza-Barron, Adsorption of trivalent chromium from aqueous solutions onto activated carbon, J. Chem. Technol. Biotechnol. 62 (1995) 64–67.
[56] D. Kratochvil, P. Pimentel, B. Volesky, Removal of trivalent and hexavalent chromium by seaweed biosorbents, Environ. Sci. Technol. 32 (1998) 2693–2698.
[57] D. Rai, B.M. Sass, D.A. Moore, Chromium(III) hydrolysis constants and solubility of chromium(III) hydroxide, Inorg. Chem. 26 (1987) 345–349.
[58] K. Lin, J. Pan, Y. Chen, R. Cheng, X. Xua, Study the adsorption of phenol from aqueous solution on hydroxyapatite nanopowders, J. Hazard. Mater. 161 (2009) 231–240.
[59] H.K. Boparai, M. Joseph, D.M. O'Carrol, Kinetics and thermodynamics of cadmium ion removal by adsorption onto nano zerovalent ironparticles, J. Hazard. Mater. 186 (2011) 458–465.
[60] Y.S. Ho, J.C.Y. Ng, G. McKay, Kinetics of pollutant sorption by biosorbents: Review, Sep. Purif. Methods 29 (2000) 189–232.
[61] Y. Li, B. Gao, T. Wu, D. Sun, X. Li, B. Wang, F. Lu, Hexavalent chromium removal from aqueous solution by adsorption on aluminum magnesium mixed hydroxide, Water Res. 43 (2009) 3067–3075.
[62] M. Danish, R. Hashim, M.N.M. Ibrahim, O. Sulaiman, Response surface methodology approach for methyl orange dye removal using optimized *Acacia mangium* wood activated carbon, Wood Sci. Technol. 48(5) (2014) 1085–1105.
[63] A.B. Albadarin, C. Mangwandi, A.H. Al-Muhtaseb, G.M. Walker, S.J. Allen, M.N.M. Ahmad, Kinetic and thermodynamics of chromium ions adsorption onto low-cost dolomite adsorbent, Chem. Eng. J. 179 (2012) 193–202.
[64] B.H. Hameed, M.I. El-Khaiary, Malachite green adsorption by rattan sawdust: Isotherm, kinetic and mechanism modeling, J. Hazard. Mater. 159 (2008) 574–579.
[65] L. Khezami, R. Capart, Removal of chromium(VI) from aqueous solution by activated carbons: Kinetic and equilibrium studies, J. Hazard. Mater. B123 (2005) 223–231.